

---

---

# Prognostic Value of Urokinase-Type Plasminogen Activator Receptor PET/CT in Head and Neck Squamous Cell Carcinomas and Comparison with <sup>18</sup>F-FDG PET/CT: A Single-Center Prospective Study

Louise M. Risør<sup>1</sup>, Malene M. Clausen<sup>2</sup>, Zaza Ujmajuridze<sup>3</sup>, Mohammed Farhadi<sup>3</sup>, Kim F. Andersen<sup>1</sup>, Annika Loft<sup>1</sup>, Jeppe Friberg<sup>2</sup>, and Andreas Kjaer<sup>1</sup>

<sup>1</sup>Department of Clinical Physiology, Nuclear Medicine, and PET and Cluster for Molecular Imaging, Copenhagen University Hospital–Rigshospitalet, and Department of Biomedical Sciences, University of Copenhagen, Copenhagen, Denmark; <sup>2</sup>Department of Clinical Oncology, Copenhagen University Hospital, Rigshospitalet, Copenhagen, Denmark; and <sup>3</sup>Department of Clinical Oncology, Næstved Hospital, Denmark

The aim of this phase II clinical trial (NCT02965001) was to evaluate the prognostic value of urokinase-type plasminogen activator receptor (uPAR) PET/CT with the novel ligand <sup>68</sup>Ga-NOTA-AE105 in head and neck cancer and compare it with <sup>18</sup>F-FDG. **Methods:** Patients with head and neck squamous cell carcinoma referred for curatively intended radiotherapy were eligible and prospectively included in this study. <sup>68</sup>Ga-uPAR and <sup>18</sup>F-FDG PET/CT were performed before initiation of curatively intended radiotherapy, and the SUV<sub>max</sub> of the primary tumor was measured on both PET/CT studies by 2 independent readers. Relapse-free survival (RFS) and overall survival (OS) were calculated, and optimal cutoffs were established for <sup>68</sup>Ga-uPAR and <sup>18</sup>F-FDG PET independently and compared using log rank and Kaplan–Meier statistics, as well as univariate and multivariate analysis in a Cox proportional-hazards model. **Results:** In total, 57 patients were included and followed for a median of 33.8 mo (range, 2.30–47.2, mo). The median SUV<sub>max</sub> of the primary tumors was 2.98 (range, 1.94–5.24) for <sup>68</sup>Ga-uPAR and 15.7 (range, 4.24–45.5) for <sup>18</sup>F-FDG. The optimal cutoffs for <sup>68</sup>Ga-NOTA-AE105 SUV<sub>max</sub> in the primary tumor were 2.63 for RFS and 2.66 for OS. A high uptake of <sup>68</sup>Ga-NOTA-AE105 (SUV<sub>max</sub> above cutoff) was significantly associated with poor RFS and OS (log-rank  $P = 0.012$  and  $P = 0.022$ ). <sup>68</sup>Ga-NOTA-AE105 uptake in the primary tumor was significantly associated with poor RFS in univariate analysis (hazard ratio [HR], 8.53 [95% CI, 1.12–64.7];  $P = 0.038$ ), and borderline-associated with OS (HR, 7.44 [95% CI, 0.98–56.4];  $P = 0.052$ ). For <sup>18</sup>F-FDG PET, the optimal cutoffs were 22.7 for RFS and 22.9 for OS. An <sup>18</sup>F-FDG SUV<sub>max</sub> above the cutoff was significantly associated with reduced RFS (log-rank  $P = 0.012$ ) and OS (log-rank  $P = 0.000$ ). <sup>18</sup>F-FDG uptake was significantly associated with reduced RFS (HR, 3.27 [95% CI, 1.237–8.66];  $P = 0.017$ ) and OS (HR, 7.10 [95% CI, 2.60–19.4];  $P < 0.001$ ) in univariate analysis. In a multivariate analysis including <sup>68</sup>Ga-uPAR SUV<sub>max</sub>, <sup>18</sup>F-FDG SUV<sub>max</sub>, TNM stage, and p16 status, only <sup>68</sup>Ga-uPAR SUV<sub>max</sub> remained significant (HR, 8.51 [95% CI, 1.08–66.9];  $P = 0.042$ ) for RFS. For OS, only TNM stage and <sup>18</sup>F-FDG remained significant. **Conclusion:** The current trial showed promising results for the use of <sup>68</sup>Ga-uPAR PET SUV<sub>max</sub> in the primary tumor to predict RFS in head and neck squamous cell carcinoma patients referred for curatively intended radiotherapy when compared with <sup>18</sup>F-FDG PET, TNM

stage, and p16 status. <sup>68</sup>Ga-uPAR PET could potentially become valuable for identification of patients suited for deescalation of treatment and risk-stratified follow-up schemes.

**Key Words:** urokinase-type plasminogen activator receptor; <sup>68</sup>Ga-NOTA-AE105; PET/CT; head and neck cancer; prognostication; risk stratification

**J Nucl Med 2022; 63:1169–1176**

DOI: 10.2967/jnumed.121.262866

**T**raditionally, head and neck squamous cell carcinoma (HNSCC) has been caused by alcohol and tobacco, but in recent years a rising incidence of oropharyngeal cancers has been associated with human papillomavirus (HPV) (1). HPV-positive tumors currently account for 63% of the oropharyngeal cancer in Western Europe and have a significantly favorable prognosis (2,3). HPV-positive and HPV-negative oropharyngeal cancers represent distinct molecular and clinical entities, and new staging guidelines reduce the stage allocation of HPV-positive tumors based on p16 immunohistochemistry as a surrogate marker of HPV-driven carcinogenesis (3,4). However, recent clinical trials investigating deescalating treatment regimens in low-risk HPV-positive oropharyngeal cancer resulted in inferior survival of the deescalating arms (5–8). To date, no reliable method of identifying candidates for deescalating treatment exists, and HPV-positive and -negative oropharyngeal cancers are treated alike (3,9).

TNM stage and HPV are the most important prognostic factors in HNSCC, but besides HPV no prognostic biomarkers are available in clinical practice. Regarding the prognostic value of <sup>18</sup>F-FDG, inconsistent results have been published (9–11).

The urokinase-type plasminogen activator receptor (uPAR) promotes cancer cell invasion by degrading the extracellular matrix and facilitates several carcinogenic processes, such as proliferation and migration (12–14). High uPAR expression has been reported in many cancer types, including HNSCC, and has been associated with aggressive disease, distant metastasis, and poor survival (14). uPAR is located on the cell surface and has limited expression in the surrounding tissue (13). Phase I studies using <sup>68</sup>Ga- and <sup>64</sup>Cu-labeled AE105 radioligands for uPAR PET in patients with different cancer types have supported the theory that uPAR is target-specific and

---

Received Aug. 9, 2021; revision accepted Nov. 16, 2021.

For correspondence or reprints, contact Andreas Kjaer (akjaer@sund.ku.dk).

Published online Dec. 2, 2021.

COPYRIGHT © 2022 by the Society of Nuclear Medicine and Molecular Imaging.

encouraged research exploring the potential of uPAR PET as a non-invasive theragnostic agent (15–17).

The aim of the current phase II clinical prospective study was to investigate the prognostic value of  $^{68}\text{Ga}$ -NOTA-AE105 uPAR PET in HNSCC patients and to compare it with  $^{18}\text{F}$ -FDG PET.

## MATERIALS AND METHODS

### Patient Population

Inclusion criteria were patients with a diagnosis of biopsy-verified cancer of the pharynx, larynx, or oral cavity, referred for curatively intended radiotherapy, who understood the given information, were able to give informed consent, and were at least 18 y old.

Exclusion criteria were pregnancy, lactation or breast feeding, an age above 85 y, obesity (body weight above 140 kg), small cancers of the larynx (stage 1A or 1B), an allergy to  $^{68}\text{Ga}$ -NOTA-AE105, metastasis on  $^{18}\text{F}$ -FDG PET/CT, other previously known cancers, and claustrophobia. Eligible patients were included after giving written informed consent. The diagnosis of HNSCC and p16 status was verified histologically before inclusion. Information on smoking, alcohol, clinical examination, treatment plan, laboratory and histologic results, medical history, and follow-up examinations was collected from patient records. Disease stage was coded according to the eighth edition of the Union for International Cancer Control classification.

The study protocol was approved by the Danish Health and Medicine Authority (EudraCT no. 2016-002082-65) and the Ethical Committee of the Capital Region of Denmark (protocol H-16039798). The study was registered at ClinicalTrials.gov (NCT02965001) and was performed in accordance with the recommendations for good clinical practice, including independent monitoring by the good-clinical-practice unit of the capital region of Denmark.

### $^{68}\text{Ga}$ -uPAR PET/CT Acquisition

According to national guidelines on treatment of HNSCC, radiotherapy is to be initiated within 11 d of the treatment decision, and  $^{18}\text{F}$ -FDG PET/CT and  $^{68}\text{Ga}$ -uPAR PET/CT were performed within this period, both as a part of the study. Since radiotherapy increases the risk of osteonecrosis following potential tooth extractions, teeth in risk of subsequent extraction are extracted prophylactically. Patients underwent a dental examination and, in the case of tooth extraction, initiation of radiotherapy was postponed until 2 wk after the procedure. In this case,  $^{18}\text{F}$ -FDG PET/CT and  $^{68}\text{Ga}$ -uPAR PET/CT were scheduled before or at least 4 d after the procedure.

All patients were injected intravenously with approximately 200 MBq (median, 191 MBq; range, 158–209 MBq) of  $^{68}\text{Ga}$ -NOTA-AE105 followed by sequential whole-body PET/CT scanning 20 min after injection. Whole-body  $^{68}\text{Ga}$ -NOTA-AE105 PET and diagnostic CT with contrast medium (skull base to proximal thigh) were performed simultaneously using an integrated whole-body PET/CT scanner (Biograph mCT, 64-slice; Siemens). The ligand was synthesized as previously described (15).

Patients were immobilized in the supine position on a flat scanner couch, with the arms placed in the standard anatomic position, and no fixating facial mask was applied. The CT scan was performed with 120 kV, 170 mAs, and a pitch of 0.8. The PET data were reconstructed with an iterative method using time of flight, point-spread function, and attenuation correction, with 2 iterations, 21 subsets, and a 2-mm gaussian filter.

### Image Analysis

Image data from the  $^{68}\text{Ga}$ -uPAR PET/CT and  $^{18}\text{F}$ -FDG PET/CT studies were analyzed by 2 certified specialists in nuclear medicine. The readers were blinded to the volumes of interest, the results of the other reader, and the patient information. Volumes of interest were visually contoured on the  $^{68}\text{Ga}$ -uPAR PET/CT images corresponding to the

localization of the primary tumor on the  $^{18}\text{F}$ -FDG PET/CT images. Uptake of the  $^{68}\text{Ga}$ -uPAR ligand and  $^{18}\text{F}$ -FDG in the volumes of interest was parameterized as  $\text{SUV}_{\text{max}}$  on the  $^{68}\text{Ga}$ -uPAR PET/CT and  $^{18}\text{F}$ -FDG PET/CT images and documented for both tracers before obtaining information on recurrence and survival.

If a patient had 2 synchronous primary HNSCCs, the tumor with the highest  $\text{SUV}_{\text{max}}$  was included in the statistical analysis. The mean  $\text{SUV}_{\text{max}}$  obtained by the 2 independent readers was included in the statistical analysis.

### Treatment and Follow-up

All patients received intensity-modulated radiotherapy with or without concomitant chemotherapy according to national guidelines (18). All patients received a prescribed dose of 66–68 Gy in 33 or 34 fractions, 6 fractions per week, and 1 patient received proton radiation. Patients with advanced disease, if assessed fit, received concomitant cisplatin weekly (40 mg/m<sup>2</sup>); all patients with normal liver and renal function test results and no neurologic symptoms received a hypoxic radiosensitizer (nimorazole) daily (1,200 mg/m<sup>2</sup>). According to national guidelines, all HNSCC patients attended a 5-y follow-up program throughout the study period, and concurrent diseases, visits to other departments, and decease of individuals were followed through the Danish personal identity number.

### Statistical Analysis

A sample size of 104 patients was calculated as needed for the study on the basis of the ability to detect an HR of 2.5 with a power of 70% ( $\beta$ , 30%), a significance level ( $\alpha$ ) of 5%, and a follow-up of 2 y. However, because of the slowdown in performing clinical studies caused by the coronavirus disease 2019 pandemic, the study was delayed, but with a longer follow-up the needed number of events was reached.

Clinical endpoints were relapse-free survival (RFS), disease-free survival (DFS), locoregional control (LRC), and overall survival (OS). RFS was defined as the time from diagnosis to any relapse of the disease at the locoregional (TN) site or distant metastasis (M) site, with deaths from other causes recorded as censoring. DFS was defined as RFS but included death of any reason as an event. Locoregional control was defined as the time from diagnosis to relapse at the locoregional site, with deaths and distant metastasis recorded as censoring. Overall survival (OS) was defined as the time from diagnosis to death of any cause. Follow-up time was calculated from the time of referral for radiotherapy until first relapse, death, or the end of follow-up (January 1, 2021).

The optimal cutoff in discrimination between favorable and poor prognosis was determined with Cutoff Finder, an R-package developed by Budczies et al. (19). Associations between biomarker expression beneath or above the cutoff and survival outcomes were visualized in Kaplan–Meier plots using the log-rank test to assess significance of differences. Hazard ratios (HRs) were estimated in univariable and multivariable Cox proportional-hazards models in which the PET parameters were included as binarized parameters according to the defined cutoffs for RFS and OS.

The number of events included in the survival analysis were 17 in RFS analysis and 16 in OS analysis. On the basis of the number of events, 4 predictors were the maximal number of explanatory variables that could reasonably be included in the final multivariable Cox model. In addition to the aim of testing the prognostic value of  $^{68}\text{Ga}$ -uPAR  $\text{SUV}_{\text{max}}$  and comparing it with  $^{18}\text{F}$ -FDG  $\text{SUV}_{\text{max}}$ , the multivariable analysis also included TNM stage and p16 status (p16-positive oropharyngeal cancer vs. all other tumors), since they are the most important nonimaging prognostic factors in HNSCC (9). Model performance was estimated using the Harrell concordance index (C-index).

The interrater reliability of SUV measurement was estimated using the intraclass correlation coefficient.

A *P* value of less than 0.05 was considered statistically significant. Statistical analyses were performed using IBM SPSS Statistics, version 22 (IBM Corp.), and R (<http://www.Rproject.org>).

## RESULTS

### Patients

In total, 57 patients recently diagnosed with HNSCC in the pharynx, larynx, or oral cavity and referred for curatively intended radiotherapy at Rigshospitalet and Næstved Hospital, Denmark, were consecutively included in the current study from December 2016 to November 2019 (Fig. 1). None of the patients experienced reactions or adverse events related to the administration of <sup>68</sup>Ga-NOTA-AE105. One patient terminated the <sup>68</sup>Ga-NOTA-AE105 (uPAR) PET/CT scan because of claustrophobia, and 2 patients were diagnosed with an unknown primary tumor of the head and neck after a lymph node biopsy and were excluded from the statistical analysis. Patient characteristics are shown in Table 1. More than half the patients (59.2%) presented with early-stage disease (stage 1 or 2), and 38.9% had no primary regional nodal disease. Moreover, 61.1% were located in the oropharynx, of which 78.7% were p16 positive. The median follow-up was 33.8 mo (range, 2.30–47.2 mo).

### Clinical Follow-up

Locoregional recurrences were histologically verified in 15 of 16 patients, serving as a reference for the study outcome. One patient did not have histologic verification of the locoregional recurrence but had active tumor at the primary site on <sup>18</sup>F-FDG

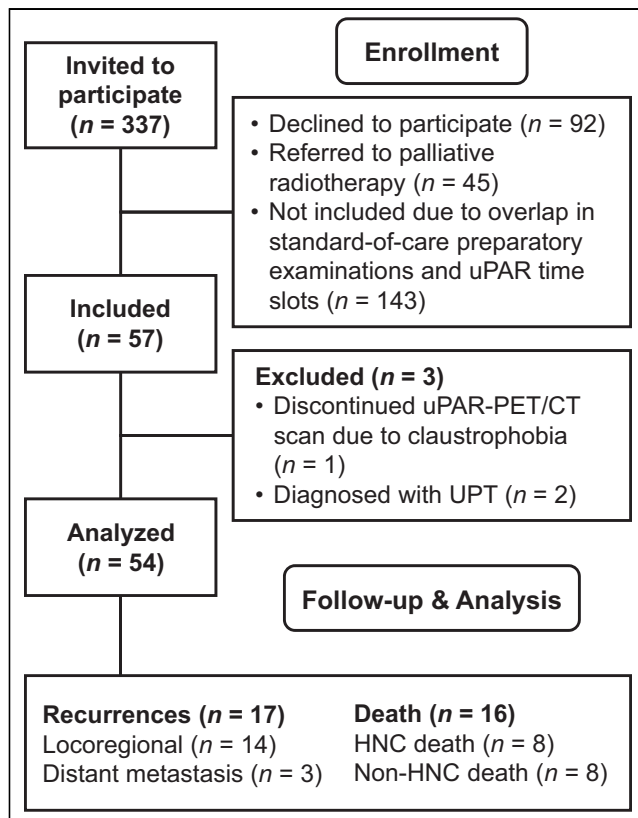


**FIGURE 1.** CONSORT (Consolidated Standards of Reporting Trials) flow diagram of inclusion process. HNC = head and neck cancer; UPT = unknown primary tumor.

**TABLE 1**  
Patient Characteristics

Characteristic	Variable	Data	%
Total patients		54	100
Sex	Male	45	83.3
	Female	9	16.7
Age	Mean	67.1	
	Range	48–84	
PS	0	51	94.4
	1	3	5.6
Smoking	Never smokers	8	14.8
	Former smokers	24	44.4
	Current smokers	22	40.7
Pack years	Mean	36.7	
	Range	0–150	
Primary site	Oral cavity	3	5.6
	Rhinopharynx	2	3.7
	Oropharynx	33	61.1
	Hypopharynx	8	14.8
	Larynx	8	14.8
P16 (oropharynx)	p16-positive	26	78.7
	p16-negative	7	21.2
EBV-positive		1	1.9
Stage*	I	12	22.2
	II	20	37.0
	III	9	16.7
	IV	13	24.1
T classification	T1	4	7.4
	T2	26	48.1
	T3	13	24.1
	T4	11	20.4
N classification	N0	21	38.9
	N1	14	25.9
	N2	19	35.2
Chemotherapy	No cisplatin	25	46.3
	Cisplatin	29	53.7
Nimorazole	No	5	9.3
	Yes	49	90.7

\*According to Union for International Cancer Control classification, eighth edition.

PS = performance status; EBV = Epstein–Barr virus.

Qualitative data are number and percentage; continuous data are mean and range.

PET/CT and histologically verified lung metastases. Biologic material from biopsy or surgery was available from all three patients with suspected distant metastasis. Consequently, we did not experience missing data regarding recurrences, and the two patients with unknown primary tumors were excluded because of missing

data from the primary tumor. No patients were lost to follow-up, and clinicopathologic information was collected before inclusion.

Seventeen patients (31.5%) were diagnosed with recurrence, 7 (13.0%) at the primary site (T site), 5 (9.3%) at the primary site and in the lymph nodes (TN site), and 2 (3.7%) in the lymph nodes (N site); 3 (5.6%) were diagnosed with distant metastases in the lungs (M site). Two of the patients were classified as having residual tumor at the 2-mo follow-up. Ten of the 17 recurrences (58.8%) were p16-negative, whereas 7 (41.2%) were p16-positive. Thirty percent (3/10) of the locoregional recurrences were p16-positive, and all cases (3/3) of distant metastasis were confirmed to be p16-positive. All 17 patients who experienced a relapse completed all fractions of the primary radiotherapy.

During follow-up, 16 patients (29.6%) died: the death was due to HNSCC in 8 (14.8%) and due to non-HNSCC causes in the other 8 (1 [1.9%] from sepsis 1 mo after treatment, 1 from exacerbation of chronic obstructive pulmonary disease, 1 from lung embolism [diagnosed and successfully operated for a recurrence before his death], 1 from discontinuation of his routine treatment of HIV followed by infection, 1 from rectal cancer, 2 from lung cancer, and 1 from unknown causes but without any sign of recurrence at the follow-up 2 mo before his death). None of the noncancer deaths had signs of recurrence at the previous follow-up. The patient who died of sepsis 1 mo after treatment before the first routine follow-up was included in the statistical analyses as not having an event. Imaging performed in the acute phase in the case of sepsis and exacerbation of chronic obstructive pulmonary disease had no sign of recurrence. Four of 6 patients whose death was due to HNSCC were p16-negative (66.7%), whereas 2 (33.3%) were p16-positive.

#### **<sup>68</sup>Ga-uPAR and <sup>18</sup>F-FDG Uptake**

The median SUV<sub>max</sub> of the primary tumors was 2.98 (range, 1.94–5.24) for <sup>68</sup>Ga-uPAR uptake and 15.7 (range, 4.24–45.5) for <sup>18</sup>F-FDG uptake (Fig. 2). The median interval between the <sup>68</sup>Ga-uPAR and <sup>18</sup>F-FDG PET/CT was 2.4 d (range, 1–4 d).

#### **Cutoffs and Kaplan–Meier Curves**

The optimal cutoffs were determined as the point with the most significant split in the Kaplan–Meier plot (log-rank test), and the corresponding HRs, including 95% CIs, were calculated (19). For <sup>68</sup>Ga-uPAR, the cut-points were 2.63 for RFS and 2.66 for OS, separating the patients into a group of 41 (75.6%) above the cutoff and 13 (24.1%) below the cutoff in RFS analysis and a group of 40 (74.1%) above and 14 (25.9%) below in OS analysis. For <sup>18</sup>F-FDG PET, the optimized cut-points were 22.7 for RFS and 22.9 for OS, separating the patients into a group of 42 (77.8%) below the cutoff and 12 (22.2%) above the cutoff in RFS analysis and a group of 43 (79.6%) below and 11 (20.4%) above in OS analysis.

Kaplan–Meier curves combined with log-rank analysis for differences showed a significant association between poor RFS (log-rank  $P = 0.012$ ) and OS (log-rank  $P = 0.02$ ) and high <sup>68</sup>Ga-uPAR SUV<sub>max</sub> above the cutoff. Similarly, <sup>18</sup>F-FDG SUV<sub>max</sub> above the cutoff was significantly associated with reduced RFS ( $P = 0.012$ ) and OS ( $P < 0.001$ ) (Fig. 3).

#### **Survival Analysis**

Univariate and multivariate analysis using Cox proportional-hazards model is summarized in Table 2. In univariate analysis, high uptake of <sup>68</sup>Ga-uPAR (above the cutoff) in the primary tumor was significantly associated with reduced RFS (HR, 8.53 [95% CI, 1.12–64.7];  $P = 0.038$ ) and was borderline-significantly associated with OS (HR, 7.44 [95% CI, 0.981–56.44];  $P = 0.052$ ). High

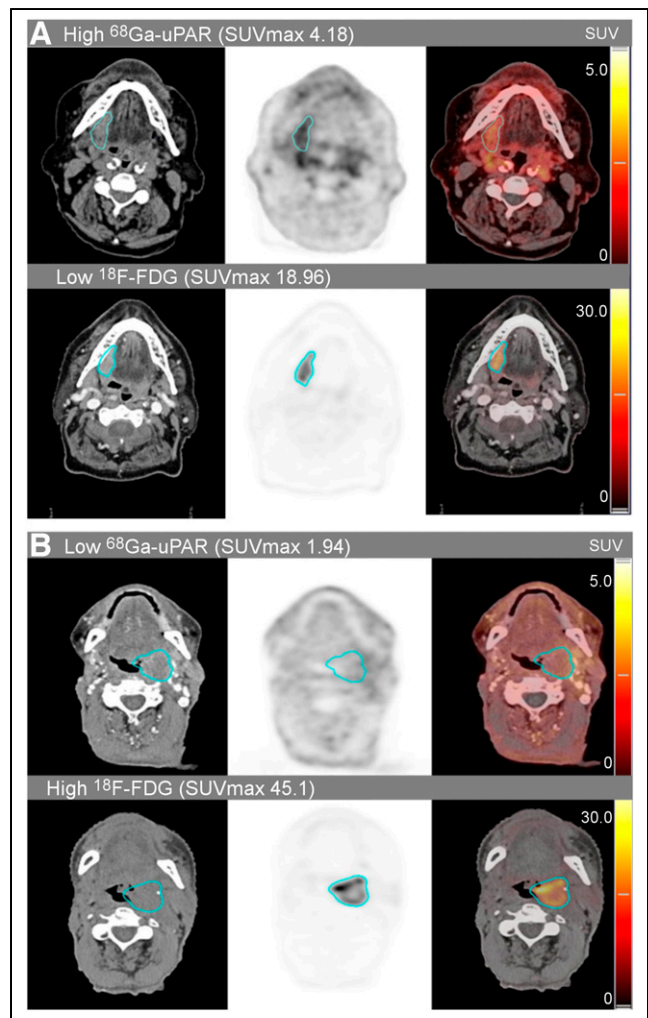


**FIGURE 2.** Delineated tumor volumes of interest in uPAR PET/CT with <sup>68</sup>Ga-NOTA-AE105 and <sup>18</sup>F-FDG-PET/CT in two cases with discordant tracer uptake. High <sup>68</sup>Ga-uPAR/low <sup>18</sup>F-FDG uptake (A) and low <sup>68</sup>Ga-uPAR/high <sup>18</sup>F-FDG uptake (B). Both cases present with stage 3 oropharyngeal cancer (T3N0M0). High and low refers to above or below the established cutoffs.

uptake of <sup>18</sup>F-FDG was significantly associated with reduced RFS (HR, 3.27 [95% CI, 1.237–8.66];  $P = 0.017$ ) and OS (HR, 7.10 [95% CI, 2.60–19.4];  $P < 0.001$ ). High TNM stage (S3 or S4) was significantly associated with both RFS (HR, 3.46 [95% CI, 1.216–9.88];  $P = 0.020$ ) and OS (HR, 6.72 [95% CI, 2.12–21.4];  $P = 0.001$ ). In multivariable analysis, including <sup>68</sup>Ga-uPAR SUV<sub>max</sub>, <sup>18</sup>F-FDG SUV<sub>max</sub>, TNM stage, and p16, only <sup>68</sup>Ga-uPAR SUV<sub>max</sub> remained significantly associated with RFS (HR, 8.50 [95% CI, 1.11–65.3];  $P = 0.040$ ), but it was not significantly associated with OS (HR, 4.58 [95% CI, 0.583–36.0];  $P = 0.148$ ). For OS, a high <sup>18</sup>F-FDG SUV<sub>max</sub> (HR, 4.986 [95% CI, 1.658–14.990];  $P = 0.004$ ) and TNM stage (HR, 3.856 [95% CI, 1.114–13.343];  $P = 0.033$ ) remained significantly associated. In disease-free survival analysis, the results reflected the fact that disease-free survival is a combination of RFS and OS events (Supplemental Table 1; supplemental materials are available at <http://jnm.snmjournals.org>). Because there were too few events, we did not have the statistical power to make conclusions on locoregional control, but the results showed the same trend as RFS.

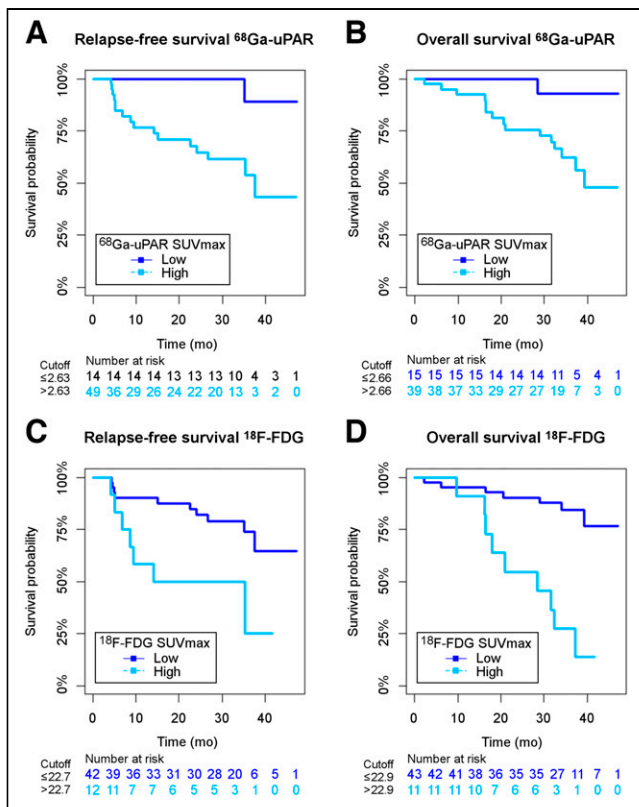


**FIGURE 3.** Kaplan–Meier plots of RFS for  $^{68}\text{Ga}$ -uPAR (A), OS for  $^{68}\text{Ga}$ -uPAR (B), RFS for  $^{18}\text{F}$ -FDG (C), and OS for  $^{18}\text{F}$ -FDG (D) stratified by corresponding  $^{68}\text{Ga}$ -uPAR and  $^{18}\text{F}$ -FDG  $\text{SUV}_{\text{max}}$  cutoffs.

In post hoc analysis, inclusion of  $^{68}\text{Ga}$ -uPAR  $\text{SUV}_{\text{max}}$  in the multivariate Cox model improved the predictive performance in RFS analysis (C-index, 0.74–0.78) and for  $^{18}\text{F}$ -FDG (C-index, 0.76–0.78). In OS analysis, inclusion of  $^{68}\text{Ga}$ -uPAR  $\text{SUV}_{\text{max}}$  improved the predictive performance (C-index, 0.81–0.84) and for  $^{18}\text{F}$ -FDG (C-index, 0.80–0.84). The C-index for a model including only TNM stage and p16 was 0.70 for RFS and 0.77 for OS.

#### $^{68}\text{Ga}$ -uPAR and $^{18}\text{F}$ -FDG Concordance

In post hoc analysis, combining  $^{68}\text{Ga}$ -uPAR PET and  $^{18}\text{F}$ -FDG into three groups (both scans low, 1 scan high/1 scan low, and both scans high) according to the established cutoffs demonstrated a concordance rate near 40% for RFS and OS and a discordance rate near 60% for RFS and OS. The distribution of the groups is shown in Table 3, and the Kaplan–Meier curves are shown in Figure 4. Overall, there was a significant difference between the groups in RFS and OS analysis (log-rank  $P = 0.001$ ). For RFS and OS, the concordantly high groups had a significantly poorer RFS than the concordantly low groups ( $P < 0.0001$ ). The group with discordant uptake (1 low/1 high) had an intermediate prognosis, with a prognosis significantly more favorable than for the concordantly high groups for both RFS and OS ( $P = 0.006$  and  $P < 0.0001$ ) but inferior to the concordantly low groups, although not reaching significance ( $P = 0.110$  and  $P = 0.069$ ).

#### Interrater Reliability

Intrater reliability in measurement of tumor  $\text{SUV}_{\text{max}}$  was good, with an intraclass correlation coefficient of 0.835 (95% CI, 0.713–0.905).

## DISCUSSION

The main finding of the current study was the ability of  $^{68}\text{Ga}$ -uPAR PET/CT with  $^{68}\text{Ga}$ -NOTA-AE105 to predict RFS in HNSCC patients referred for curatively intended radiotherapy. In univariate analysis,  $^{18}\text{F}$ -FDG- $\text{SUV}_{\text{max}}$  also predicted RFS; however, in a multivariate analysis including  $^{68}\text{Ga}$ -uPAR  $\text{SUV}_{\text{max}}$ ,  $^{18}\text{F}$ -FDG- $\text{SUV}_{\text{max}}$ , TNM stage, and p16 immunohistochemistry, only  $^{68}\text{Ga}$ -uPAR  $\text{SUV}_{\text{max}}$  remained significant.

Accordingly, we demonstrated that a primary tumor  $^{68}\text{Ga}$ -uPAR PET  $\text{SUV}_{\text{max}}$  cutoff could be established for identification of high- and low-risk groups of HNSCC patients referred for curatively intended radiotherapy. The PET parameter  $\text{SUV}_{\text{max}}$  is simple to obtain and is the most frequently reported and most reproducible PET uptake metric in the literature (20).

The large proportion (8/16, 50%) of non-HNC-related deaths found in our study may explain why  $^{68}\text{Ga}$ -uPAR PET was not able to predict OS. The poor general health status of many HNSCC patients is known to result in a high number of non-HNSCC deaths due to competing risks after tobacco and alcohol consumption (21). However, our study was not powered to evaluate  $^{68}\text{Ga}$ -uPAR PET in predicting HNSCC-related deaths.

Since uPAR expression takes part in the tumor invasion and metastasis process (12,14), it is not surprising that high levels of uPAR PET are related to relapse. Previous phase I clinical trials of  $^{68}\text{Ga}$ -uPAR PET (16,17,22), as well as an array of preclinical studies (13,23–26), have demonstrated that  $^{68}\text{Ga}$ -uPAR PET indeed visualizes uPAR expression.

$^{18}\text{F}$ -FDG PET  $\text{SUV}_{\text{max}}$  is the most common and best-characterized PET uptake metric and is a proposed prognostic marker in various cancers. Therefore, in our study we predefined  $^{18}\text{F}$ -FDG PET  $\text{SUV}_{\text{max}}$  for comparison. For HNSCC, several studies have concluded that  $^{18}\text{F}$ -FDG PET  $\text{SUV}_{\text{max}}$  does hold prognostic information, but results have been inconsistent. Most of the studies have been retrospective cohort studies, and there has been concern that  $^{18}\text{F}$ -FDG is simply a surrogate marker of known clinical risk factors, especially tumor size (10,11). However, our results support the evidence that  $\text{SUV}_{\text{max}}$  is a significant predictor of patient outcome for both  $^{68}\text{Ga}$ -uPAR and  $^{18}\text{F}$ -FDG in univariate analysis.

$^{18}\text{F}$ -FDG is not tumor-specific, and various image interpretation pitfalls exist due to physiologic uptake and the complex anatomy of the head and neck (27). We found that  $^{18}\text{F}$ -FDG PET  $\text{SUV}_{\text{max}}$  could predict OS but not RFS in the multivariate model.  $^{68}\text{Ga}$ -uPAR PET remained significant regarding RFS in the multivariate model, but not  $^{18}\text{F}$ -FDG PET, demonstrating that the prognostic information obtained with  $^{68}\text{Ga}$ -uPAR is different from that obtained with  $^{18}\text{F}$ -FDG PET. The two tracers may be used for different purposes and complement each other in providing a detailed noninvasive whole-tumor characterization (28–30).  $^{68}\text{Ga}$ -uPAR and  $^{18}\text{F}$ -FDG concordance could supply additional information to a future risk stratification of low (both low), intermediate (1 low/1 high), and high-risk patients (both high) for personalized treatment and follow-up strategies.

More recent  $^{18}\text{F}$ -FDG PET uptake metrics—metabolic tumor volume and total lesion glycolysis—have shown promising prognostic results, and inclusion of such parameters in future and higher-phase studies could be of interest (31). Nonetheless, these parameters have several limitations, and no consensus regarding volume segmentation and threshold has been established (31). In  $^{68}\text{Ga}$ -uPAR PET prognostication, we believe that  $\text{SUV}_{\text{max}}$  is the relevant metric for characterization of the most aggressive phenotype

**TABLE 2**  
Cox Proportional Hazards Model for RFS and OS in Relation to Clinicopathologic Parameters and <sup>68</sup>Ga-uPAR and <sup>18</sup>F-FDG Uptake

Parameter	Variable	n	RFS						OS							
			Univariate analysis			Multivariate analysis			Univariate analysis			Multivariate analysis				
			HR	95% CI	P	HR	95% CI	P	HR	95% CI	P	HR	95% CI	P		
Sex	Women	9														
	Men	45	3.666	0.486–27.657	0.208							3.109	0.410–23.578	0.273		
Age*																
	<30 pack years	29	0.993	0.943–1.046	0.802							1.035	0.984–1.090	0.184		
Smoking	>30 pack years	25	1.129	0.433–2.947	0.804							3.072	1.060–8.906	0.039		
TNM stage	S1–2	32														
	S3–4	22	3.458	1.211–9.875	0.020	2.702	0.827–8.832	0.100	6.724	2.117–21.355	0.001	4.309	1.239–14.984	0.022		
p16	Positive	26														
	Negative	28	2.361	0.864–6.456	0.094	1.006	0.331–3.064	0.991	4.615	1.314–16.212	0.017	1.712	0.438–6.691	0.440		
<sup>68</sup> Ga-uPAR	<Cutoff	13														
	>Cutoff	41	8.530	1.124–64.743	0.038	8.511	1.082–66.949	0.042	7.439	0.981–56.415	0.052	4.584	0.583–36.044	0.148		
<sup>18</sup> F-FDG	<Cutoff	42														
	>Cutoff	12	3.266	1.231–8.662	0.017	2.240	0.724–6.933	0.162	7.098	2.602–19.360	0.000	4.285	1.362–13.479	0.013		

\*Age was included as continuous covariate.

**TABLE 3**

Distribution of Patients According to Cutoffs for <sup>68</sup>Ga-uPAR PET and <sup>18</sup>F-FDG PET SUV<sub>max</sub> for RFS and OS

Parameter	uPAR low	uPAR high	Total
<b>RFS concordance</b>			
<sup>18</sup> F-FDG low	12 (22.2%)	30 (55.6%)	42 (77.8%)
<sup>18</sup> F-FDG high	2 (3.7%)	10 (18.5%)	12 (22.2%)
Total	14 (25.9%)	40 (74.1%)	54 (100%)
<b>OS concordance</b>			
<sup>18</sup> F-FDG low	12 (22.2%)	31 (57.4%)	43 (79.6%)
<sup>18</sup> F-FDG high	2 (3.7%)	9 (16.7%)	12 (20.4%)
Total	14 (25.9%)	40 (74.1%)	54 (100%)

within the tumor and as a predictor of prognosis rather than a measure of volume.

The current study represents a first proof of concept in a moderately sized population. Larger future prospective (phase III) studies are needed to establish the exact cutoffs, which may also depend on the exact composition of the population. Nevertheless, with the current SUV<sub>max</sub> cutoff at 2.63, we identified the 25% of patients with a low risk of recurrence. Because of the considerable toxicity associated with chemoradiotherapy, initiatives to deescalate the treatment for selected patients are being explored, and <sup>68</sup>Ga-uPAR may assist with a reliable identification of such low-risk patients (7).

Moreover, there is considerable variation in surveillance strategies after treatment of head and neck cancer (32). Routine imaging is not standardized, and patients often request fewer follow-up visits (33). If results are validated, <sup>68</sup>Ga-uPAR PET may contribute to the development of risk-stratified follow-up schedules.

In past decades, research in optimizing treatment for HNSCC patients has focused on the geometric precision of radiotherapy, but a shift toward biologic precision has begun. The prognostic strength of <sup>68</sup>Ga-uPAR PET is the quantitative readout from tumor lesions and not a visual delineation, as some tumors may have low or almost no uptake. Accordingly, <sup>68</sup>Ga-uPAR PET will not replace <sup>18</sup>F-FDG PET as a diagnostic tool. In addition, <sup>68</sup>Ga-uPAR PET/CT may become an important companion diagnostic for selection of patients eligible for uPAR-targeted optically guided surgery using a

uPAR-targeted optical probe or uPAR-targeted radionuclide therapy, as well as for planning of external-radiation therapy with customization of uPAR-targeted dose delivery of intensity-modulated radiotherapy in patients with high tumor uptake (23,34–37).

**CONCLUSION**

The current trial evaluating the prognostic impact of <sup>68</sup>Ga-uPAR PET/CT using <sup>68</sup>Ga-NOTA-AE105 showed that <sup>68</sup>Ga-uPAR PET SUV<sub>max</sub> can predict RFS in HNSCC patients referred for curatively intended radiotherapy. In a multivariate analysis including <sup>68</sup>Ga-uPAR SUV<sub>max</sub>, <sup>18</sup>F-FDG SUV<sub>max</sub>, TNM stage, and p16 status, only <sup>68</sup>Ga-uPAR SUV<sub>max</sub> remained significant for RFS. For OS, TNM stage and <sup>18</sup>F-FDG SUV<sub>max</sub> were significant.

**DISCLOSURE**

Andreas Kjaer is an inventor on a patent for the composition of matter of uPAR PET (WO 2014086364) and a cofounder of Cura-sight, which has licensed the uPAR PET technology. This project received funding from the European Union’s Horizon 2020 research and innovation program under grants 670261 (ERC advanced grant) and 668532 (Click-It), the Lundbeck Foundation, the Novo Nordisk Foundation, the Innovation Fund Denmark, the Danish Cancer Society, the Arvid Nilsson Foundation, the Neye Foundation, the Research Foundation of Rigshospitalet, the Danish National Research Foundation (grant 126), the Research Council of the Capital Region of Denmark, the Danish Health Authority, the John and Birthe Meyer Foundation, and the Danish Council for Independent Research. Andreas Kjaer is a Lundbeck Foundation professor. No other potential conflict of interest relevant to this article was reported.

**KEY POINTS**

**QUESTION:** What is the prognostic value of the novel ligand <sup>68</sup>Ga-NOTA-AE105 for uPAR PET/CT in HNSCC?

**PERTINENT FINDINGS:** High primary-tumor uptake of the uPAR PET tracer was associated with poor RFS in HNSCC patients, whereas high primary-tumor uptake of the <sup>18</sup>F-FDG PET tracer was associated with poor OS.

**IMPLICATIONS FOR PATIENT CARE:** uPAR PET/CT offers a potential tool for clinicians to select low-risk HNSCC patients for deescalated treatment regimens to avoid unnecessary toxicity and for a risk-stratified follow-up schedule.

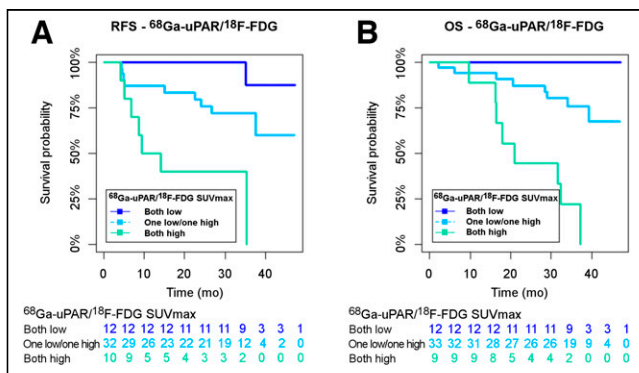


**FIGURE 4.** Kaplan-Meier plots of RFS (A) and OS (B) for concordant and discordant groups: <sup>68</sup>Ga-uPAR and <sup>18</sup>F-FDG both low (dark blue); 1 low/1 high (turquoise); and both high (green).

**REFERENCES**

- Chaturvedi AK, Engels EA, Pfeiffer RM, et al. Human papillomavirus and rising oropharyngeal cancer incidence in the United States. *J Clin Oncol*. 2011;29:4294–4301.
- Mehanna H, Franklin N, Compton N, et al. Geographic variation in human papillomavirus-related oropharyngeal cancer: data from 4 multinational randomized trials. *Head Neck*. 2016;38(suppl 1):E1863–E1869.
- Albers AE, Qian X, Kaufmann AM, Coordes A. Meta analysis: HPV and p16 pattern determines survival in patients with HNSCC and identifies potential new biologic subtype. *Sci Rep*. 2017;7:16715.
- O’Sullivan B, Huang SH, Su J, et al. Development and validation of a staging system for HPV-related oropharyngeal cancer by the International Collaboration on Oropharyngeal cancer Network for Staging (ICON-S): a multicentre cohort study. *Lancet Oncol*. 2016;17:440–451.
- Jakobsen KK, Gronhoj C, Jensen DH, et al. Increasing incidence and survival of head and neck cancers in Denmark: a nation-wide study from 1980 to 2014. *Acta Oncol*. 2018;57:1143–1151.

6. Craig SG, Anderson LA, Schache AG, et al. Recommendations for determining HPV status in patients with oropharyngeal cancers under TNM8 guidelines: a two-tier approach. *Br J Cancer*. 2019;120:827–833.
7. Gillison ML, Trotti AM, Harris J, et al. Radiotherapy plus cetuximab or cisplatin in human papillomavirus-positive oropharyngeal cancer (NRG Oncology RTOG 1016): a randomised, multicentre, non-inferiority trial. *Lancet*. 2019;393:40–50.
8. Mehanna H, Robinson M, Hartley A, et al. Radiotherapy plus cisplatin or cetuximab in low-risk human papillomavirus-positive oropharyngeal cancer (De-ESCA-LaTE HPV): an open-label randomised controlled phase 3 trial. *Lancet*. 2019;393:51–60.
9. Burd EM. Human papillomavirus laboratory testing: the changing paradigm. *Clin Microbiol Rev*. 2016;29:291–319.
10. Clausen MM, Vogelius IR, Kjaer A, Bentzen SM. Multiple testing, cut-point optimization, and signs of publication bias in prognostic FDG-PET imaging studies of head and neck and lung cancer: a review and meta-analysis. *Diagnostics (Basel)*. 2020;10:1030.
11. Rasmussen JH, Vogelius IR, Fischer BM, et al. Prognostic value of <sup>18</sup>F-fluorodeoxyglucose uptake in 287 patients with head and neck squamous cell carcinoma. *Head Neck*. 2015;37:1274–1281.
12. Dass K, Ahmad A, Azmi AS, Sarkar SH, Sarkar FH. Evolving role of uPA/uPAR system in human cancers. *Cancer Treat Rev*. 2008;34:122–136.
13. Persson M, Kjaer A. Urokinase-type plasminogen activator receptor (uPAR) as a promising new imaging target: potential clinical applications. *Clin Physiol Funct Imaging*. 2013;33:329–337.
14. Mekkawy AH, Pourgholami MH, Morris DL. Involvement of urokinase-type plasminogen activator system in cancer: an overview. *Med Res Rev*. 2014;34:918–956.
15. Skovgaard D, Persson M, Brandt-Larsen M, et al. Safety, dosimetry, and tumor detection ability of <sup>68</sup>Ga-NOTA-AE105: first-in-human study of a novel radioligand for uPAR PET imaging. *J Nucl Med*. 2017;58:379–386.
16. Skovgaard D, Persson M, Kjaer A. Urokinase plasminogen activator receptor-PET with <sup>68</sup>Ga-NOTA-AE105: first clinical experience with a novel PET ligand. *PET Clin*. 2017;12:311–319.
17. Persson M, Skovgaard D, Brandt-Larsen M, et al. First-in-human uPAR PET: imaging of cancer aggressiveness. *Theranostics*. 2015;5:1303–1316.
18. *Radiotherapy Guidelines 2020*. DAHANCA; 2020:1–57.
19. Budczies J, Klauschen F, Sinn BV, et al. Cutoff Finder: a comprehensive and straightforward web application enabling rapid biomarker cutoff optimization. *PLoS One*. 2012;7:e51862.
20. Wahl RL, Jacene H, Kasamon Y, Lodge MA. From RECIST to PERCIST: evolving considerations for PET response criteria in solid tumors. *J Nucl Med*. 2009;50(suppl 1):122S–150S.
21. Gillison ML, Zhang Q, Jordan R, et al. Tobacco smoking and increased risk of death and progression for patients with p16-positive and p16-negative oropharyngeal cancer. *J Clin Oncol*. 2012;30:2102–2111.
22. Skovgaard D, Persson M, Kjaer A. Imaging of prostate cancer using urokinase-type plasminogen activator receptor PET. *PET Clin*. 2017;12:243–255.
23. Persson M, Madsen J, Ostergaard S, et al. Quantitative PET of human urokinase-type plasminogen activator receptor with <sup>64</sup>Cu-DOTA-AE105: implications for visualizing cancer invasion. *J Nucl Med*. 2012;53:138–145.
24. Persson M, Hosseini M, Madsen J, et al. Improved PET imaging of uPAR expression using new <sup>64</sup>Cu-labeled cross-bridged peptide ligands: comparative in vitro and in vivo studies. *Theranostics*. 2013;3:618–632.
25. Persson M, Liu H, Madsen J, Cheng Z, Kjaer A. First <sup>18</sup>F-labeled ligand for PET imaging of uPAR: in vivo studies in human prostate cancer xenografts. *Nucl Med Biol*. 2013;40:618–624.
26. Persson M, El Ali HH, Binderup T, et al. Dosimetry of <sup>64</sup>Cu-DOTA-AE105, a PET tracer for uPAR imaging. *Nucl Med Biol*. 2014;41:290–295.
27. Purohit BS, Ailianou A, Dulguerov N, Becker CD, Ratib O, Becker M. FDG-PET/CT pitfalls in oncological head and neck imaging. *Insights Imaging*. 2014;5:585–602.
28. Marcu LG, Reid P, Bezak E. The promise of novel biomarkers for head and neck cancer from an imaging perspective. *Int J Mol Sci*. 2018;19:2511.
29. Song IH, Noh Y, Kwon J, et al. Immuno-PET imaging based radioimmunotherapy in head and neck squamous cell carcinoma model. *Oncotarget*. 2017;8:92090–92105.
30. Christensen A, Kiss K, Lelkaitis G, et al. Urokinase-type plasminogen activator receptor (uPAR), tissue factor (TF) and epidermal growth factor receptor (EGFR): tumor expression patterns and prognostic value in oral cancer. *BMC Cancer*. 2017;17:572.
31. Rijo-Cedeño J, Mucientes J, Seijas Marcos S, et al. Adding value to tumor staging in head and neck cancer: the role of metabolic parameters as prognostic factors. *Head Neck*. 2021;43:2477–2487.
32. Wong WL. PET-CT for staging and detection of recurrence of head and neck cancer. *Semin Nucl Med*. 2021;51:13–25.
33. Trindade A, Kothari P, Andreou Z, Hewitt RJ, O'Flynn P. Follow-up in head and neck cancer: patients' perspective. *Int J Health Care Qual Assur*. 2012;25:145–149.
34. Christensen A, Juhl K, Persson M, et al. uPAR-targeted optical near-infrared (NIR) fluorescence imaging and PET for image-guided surgery in head and neck cancer: proof-of-concept in orthotopic xenograft model. *Oncotarget*. 2017;8:15407–15419.
35. Ling CC, Humm J, Larson S, et al. Towards multidimensional radiotherapy (MD-CRT): biological imaging and biological conformality. *Int J Radiat Oncol Biol Phys*. 2000;47:551–560.
36. Atallah I, Millet C, Henry M, et al. Near-infrared fluorescence imaging-guided surgery improves recurrence-free survival rate in novel orthotopic animal model of head and neck squamous cell carcinoma. *Head Neck*. 2016;38(suppl 1):E246–E255.
37. Persson M, Madsen J, Ostergaard S, Ploug M, Kjaer A. <sup>68</sup>Ga-labeling and in vivo evaluation of a uPAR binding DOTA- and NODAGA-conjugated peptide for PET imaging of invasive cancers. *Nucl Med Biol*. 2012;39:560–569.